

Combining Multi-Variate Statistics and Speckle Reduction for Line Detection in Multi-Channel SAR Images

Dirk Borghys ^{*}, Christiaan Perneel ^{*}, Aleksandra Pizurica [†] and Wilfried Philips [†]

^{*} Royal Military Academy, Signal & Image Centre,
Renaissancelaan 30, B-1000 Brussels, Belgium

[†] Dept of Telecommunications and Information Processing, University of Ghent,
Sint-Pietersnieuwstraat 41, B-9000 Gent, Belgium

ABSTRACT

The current paper focuses on the detection of linear objects (e.g. roads, rivers, tree lines, etc.) in multi-frequency polarimetric SAR images. We obtained sets of full-polarimetric P-band and L-band and VV-polarised C- and X-band images. The images cover the same region but have a different spatial resolution. We also obtained transformation matrices that relate the slant-range coordinates to geocoded coordinates for each frequency band. The detection of linear features is performed on each of the slant-range images and the results are then geocoded and fused. In SAR images, for deciding whether a line passes through a given point, a relatively large neighbourhood has to be considered because of the speckle. Normally a set of rectangles is scanned over the image and at each point the statistics of the pixels inside the different rectangles are compared to decide whether a line is present. For single-channel data, a line detector is constructed from the Touzi edge detector. For polarimetric data, we use a multi-variate hypothesis test. Because of the difference in spatial resolution and information content of the 4 frequency bands, results are improved by fusing the individual results from the different bands. On the other hand, the synergy with speckle reduction is also examined. Without speckle reduction, large scanning rectangles need to be used for the line detection because of the presence of the speckle. If speckle reduction is applied prior to line detection, smaller rectangles can be used. The former approach allows to detect lines that show a lower contrast while the latter allows to find smaller details and achieves a higher spatial accuracy. The proposed method was applied to one of the sets of images and results are shown and evaluated.

Keywords: Multi-Channel SAR Images, Polarimetric SAR, Line Detection, Road Detection

1. INTRODUCTION

In this paper we present an approach for the detection of linear objects in multi-channel SAR images. In general, traditional image processing algorithms fail in SAR images because of an interference phenomenon, called speckle, which results in very noisy appearance of the images. Specific SAR image processing methods, which take into account the properties of the speckle, have been developed since the eighties. For edge- and line detection, existing methods are focussed on multi-look, mono-polarisation, single-frequency images (e.g.^{1,2} for line detection). Current airborne SAR systems and future satellite systems acquire multi-channel SAR data, i.e. full-polarimetric and/or multi-frequency data, because such data contain a lot more information. For edge- and line detection in polarimetric images it is possible to use methods based on multi-variate statistics.³ In this paper we try to find linear objects in a set of multi-channel SAR images. We have P- and L-band full-polarimetric images and VV-polarised C- and X-band images of the same region. The different bands do not have the same spatial resolution. Geocoding information is also available. We apply a line detector to each band separately and then geocode and combine the results. For the polarimetric images we use the multi-variate detector, for the single-channel images we use a detector based on the touzi edge detector. We also investigate the synergy between line detection and speckle reduction. The speckle reduction scheme⁴ that is used

Further author information: Send correspondence to Dirk.Borghys@elec.rma.ac.be

combines a context-based locally adaptive wavelet shrinkage and Markov Random Fields to limit blurring of edges and incorporate prior knowledge about edge configurations. For the line detection after speckle reduction the multi-variate method is used for the polarimetric images and another statistical hypothesis test is used for the single-polarisation images. The results are geocoded and a method to combine the results from different bands is proposed. The method was applied to detect lines of trees and shrubs using a detector for bright lines and to detect roads and rivers using a dark bar detector. The results at different stages of the method are evaluated using Receiver-Operator Characteristic (ROC) curves. The ground-truth was manually delimited on a high-resolution visual image of the same region.

2. OVERVIEW OF THE IMAGE SET

For this project, the German Aerospace Agency, DLR, provided us with E-SAR images with 4 different frequencies. The P- and L-band images are full-polarimetric, while for C - and X-band only the VV-polarisation is available. The images are delivered as slant-range, single-look complex (SLC) data. All images were acquired from parallel flight paths and cover approximately the same region. However the pixel spacing of the images of different bands is not the same. Together with the SLC images we received geocoding matrices that enable one to find the ground coordinates of each point in the SLC images. These were obtained by the German Space Agency DLR by geocoding the SAR image using a DEM of the region. Table 1 gives an overview of the principal characteristics of the images. In fig. 1 the VV-polarised component of part of the geocoded image is shown for the four frequencies. The images were rescaled such that they subjectively present a good overall contrast.

Band	Wavelength	Polarisation	Size [$W \times H$]	Pixel Spacing [$Range \times Azimuth$]
P	70 cm	HH,HV,VV	1410 \times 5790	1.50m \times 0.70m
L	23 cm	HH,HV,VV	1452 \times 9598	1.50m \times 0.43m
C	5.6 cm	VV	1456 \times 11350	1.50m \times 0.36m
X	3 cm	VV	1455 \times 11753	1.50m \times 0.35m

Table 1. Overview of the principal characteristics of the image set

3. LINE DETECTION IN SAR IMAGES

3.1. General Principle

Florence Tupin^{1,5} has proposed a method for constructing a bar or line detector for SAR images from edge detectors. The idea is the following: In order to determine whether a road passes through a given point, in a given direction, a set of rectangles is defined around the point and some statistics are estimated in each of the rectangles. The decision is based on a difference between the values of the statistics obtained in the different rectangles. For line detection three rectangles are used. The middle one is centered on the current point and is usually narrower than the two others. In fig. 2 the principle is represented schematically.

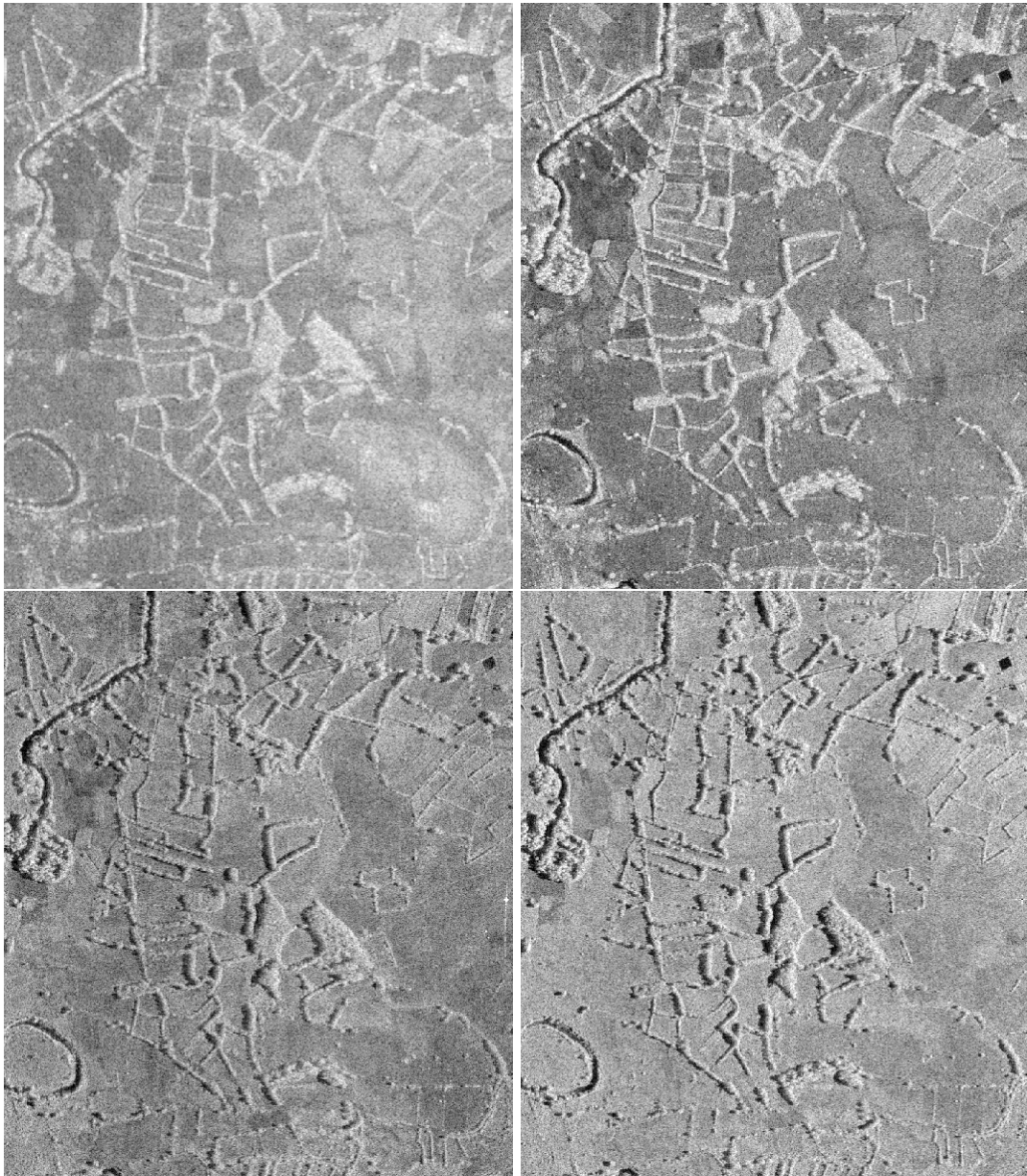


Figure 1. Overview of original VV-polarised E-SAR images (©DLR): P-band (top left), L-band (top right), C-band (bottom left) and X-band (bottom right)

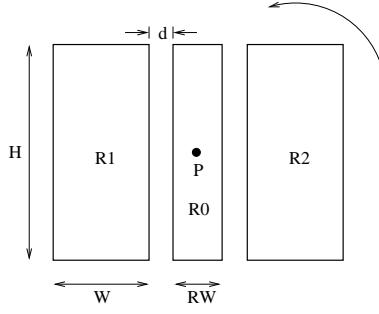


Figure 2. General Principle for Line Detection in SAR Images

In order to detect whether a line in a given orientation passes through the point P the statistics of the two outer rectangles are compared with those in the middle one. The response of the detector is the response corresponding to the smallest difference in statistics. This allows to distinguish edges from lines.

Let F_{R_i, R_j} be a measurement of the statistical difference between rectangle R_i and R_j , the line detector's response r will then be given by:

$$r = \min(F_{R_0, R_1}, F_{R_0, R_2}) \quad (1)$$

The way F_{R_i, R_j} is obtained depends on the method that is used. The next subsections describe the methods that were used in this article. In fact F_{R_i, R_j} is a measurement for the edge strength between the two rectangles R_i and R_j .

In the design of the detector's parameters the width of the central rectangle has to be chosen such that it corresponds to the possible widths of the lines to be detected. The gaps between the middle and outer rectangles allow to reduce the correlation between the three rectangles as well as to build-in a tolerance for the possible widths and orientations of the lines.

The method described above gives a response for one possible line orientation. The test should be repeated for different orientations of the scanning rectangles and the results combined. We used 16 different orientations. For the combination of the line response for different orientations the maximum operator was used. This results in a value for the line strength as well as the corresponding line orientation in each pixel.

3.2. Line detector based on the Touzi edge detector

Tupin¹ derived a line detector from the ratio edge detector which was introduced by Bovik⁶ and statistically studied by Touzi et al.⁷ The Touzi edge detector is based on the ratio of averages in intensity images. The edge detector response F_{R_i, R_j} between rectangle i and j is defined as:

$$F_{R_i, R_j} = 1 - \min\left(\frac{\mu_i}{\mu_j}, \frac{\mu_j}{\mu_i}\right), \quad (2)$$

with μ_i the empirical mean of rectangle i . We refer to the work of F. Tupin^{1, 5} for a statistical study of the properties of this line detector. This detector is applied to intensity images.

3.3. Line detector based on the Hotellings T^2 test

For multi-channel images, it is possible to construct a line detector from an edge detector based on multi-variate statistical hypothesis tests.⁸ Multi-variate method treat the different channels at the same time and take into account the correlation between the channels, which is very important in polarimetric SAR images. The multi-variate method used is the *Hotelling T^2 test* for the difference of means. The null hypothesis H_0 is that the samples from the two scanning rectangles are drawn from populations with the same mean. The alternative hypothesis H_1 is that the mean of one population is different from that of the other. The actual test-statistic is defined as:

$$T^2 = \frac{n_i n_j (\bar{\mathbf{X}}_i - \bar{\mathbf{X}}_j)^t [\mathbf{C}_{ij}]^{-1} (\bar{\mathbf{X}}_i - \bar{\mathbf{X}}_j)}{n_i + n_j} \quad (3)$$

with $\bar{\mathbf{X}}_i$ and $\bar{\mathbf{X}}_j$ the vectors of averages of the values in the respective scanning rectangles i ($i=1,2$ or 3) and n_i, n_j is the number of observations used in the respective scanning rectangle to estimate the test statistics. Each element of the vector represents the average for one polarisation. $[\mathbf{C}_{ij}]$ is the pooled covariance matrix defined as:

$$[\mathbf{C}_{ij}] = \frac{(n_i - 1)[\mathbf{C}_i] + (n_j - 1)[\mathbf{C}_j]}{n_i + n_j - 2} \quad (4)$$

with $[\mathbf{C}_i]$ and $[\mathbf{C}_j]$ respectively the polarimetric covariance matrix in the two scanning rectangles. The significance of T^2 is determined by using the fact that in the null-hypothesis of equal population means the transformed statistic

$$F_{R_i, R_j} = \frac{(n_i + n_j - p - 1)T^2}{(n_i + n_j - 2)p} \sim F(p, n_i + n_j - p - 1) \quad (5)$$

The test-statistic follows an F distribution with degrees of freedom p and $(n_i + n_j - p - 1)$. p is the number of images that is used. For a single-band, full-polarimetric image $p = 3$.

The log-intensity image is the best candidate for comparing regions on the basis of this test because differences in radar reflectivity appear in these image purely as variations of means and because the form of the distribution is independent of the radar reflectivity.

The detector based on the Hotellings T^2 test can be applied to multi-channel images with or without speckle reduction.

3.4. Line detector based on a Student-t test

The Touzi detector is an optimal detector for single-channel SAR intensity images containing speckle. If the speckle has been reduced, a classical statistical hypothesis test can be used too. We developed a method analogous to the Hotellings test and very similar to the Student t-test for uni-variate difference of means.⁹ If the null-hypothesis H_0 is valid, i.e. if there is no edge between the two regions R_i and R_2 , their theoretical averages is the same and a statistic D_{12} can be defined which follows a normal distribution:

$$F_{R_i, R_j} = \frac{\bar{x}_i - \bar{x}_j}{\sqrt{\frac{\sigma_{x_i}^2}{n_1} + \frac{\sigma_{x_j}^2}{n_2}}} \sim \mathcal{N}(0, 1) \quad (6)$$

This detector is applied to log-intensity images.

3.5. Detection of roads or waterways

The surface of roads or rivers is usually smooth compared to the wavelength of the radar. The Rayleigh criterion considers a surface to be smooth if its average height variations ΔH fulfill:

$$\Delta H \ll \frac{\lambda}{8 \cos(\theta)} \quad (7)$$

with λ the wavelength of the radar and θ the local incidence angle. For the E-SAR system the incidence angle varies from 25° to 57° over the swath. Table 2 presents the limits for the Rayleigh criterion for the 4 frequency bands of the E-SAR system.

Band	Wavelength	Limits for Rayleigh Criterion
P	70 cm	10 cm - 16 cm
L	23 cm	3 cm - 5 cm
C	5.6 cm	0.7 cm - 1.3 cm
X	3 cm	0.4 cm - 0.6 cm

Table 2. Limits for the Rayleigh criterion for the different bands of the E-SAR system

For P- and L-band the surface of a road will thus behave as a mirror; all signal is reflected away from the radar and the image intensity is purely due to thermal noise. For X- and C-band the roads will still appear dark, but a small part of the energy is reflected towards the radar. In many cases roads will thus appear very dark in the SAR image. However, due to the direct environment of the road and in particular the presence of shrubs, trees, ditches boarding the road, double bounce reflections can occur and the road will appear very bright.⁵ This effect only occurs for roads that are almost perpendicular to the viewing direction of the radar. Roads will thus either appear very dark or very bright. An extra condition in the road detection algorithm can thus be based on a comparison of the average greyvalue of the centre rectangle A_{R_o} with the one found in the two outer rectangles A_{R_1} and A_{R_2} . The response r of the detector for dark lines will thus be:

$$r = \begin{cases} \text{MIN}(F_{R_o,R_1}, F_{R_o,R_2}) & \text{if } (A_{R_o} < A_{R_1}) \text{ and } (A_{R_o} < A_{R_2}) \\ 0 & \text{otherwise} \end{cases} \quad (8)$$

For multi-channel images, the condition on the averages is imposed on each channel separately.

A detector of dark lines will detect roads, rivers and radar shadows; a detector of bright lines will mainly detect double bounce scattering from either trees or buildings.

4. SPECKLE REDUCTION

Standard speckle reduction methods tend to blur the image. In particular edges are smoothed and strong isolated scatterers are removed. Because these two features are very important, a speckle reduction method was developed to preserve edges and isolated strong scatterers. The method was developed by A. Pizurica⁴ and is based on a context-based locally adaptive wavelet shrinkage. The idea is to estimate the statistical distributions of the wavelet coefficients representing mainly noise and representing useful edges. In particular, it was noted that in SAR intensity images, the magnitudes of the wavelet coefficients representing mainly noise follow an exponential distribution while the magnitudes of the wavelet coefficients representing mainly useful signal follow a Gamma distribution. This information is used to find a threshold that allows to distinguish the useful signal from the noise. Prior knowledge about possible edge configurations is introduced using a Markov Random Field. More details about the speckle reduction method can be found in.^{4,10} In fig. 3 a typical result of the speckle reduction is shown and compared to the classical Gamma-MAP filter.¹¹

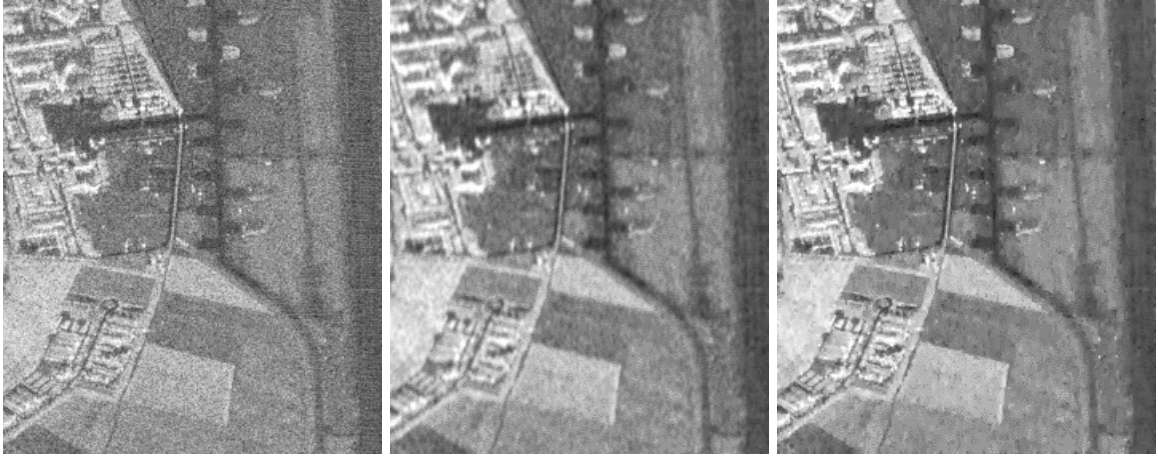


Figure 3. Results of speckle reduction. Left: Original image (L-band, HH-polarised E-SAR image provided by the German Aerospace Agency DLR), Centre: results of Gamma-MAP filter, Right: results of described method)

5. STRATEGY FOR LINE DETECTION IN MULTI-CHANNEL SAR IMAGES

5.1. Global Overview

Preliminary tests have shown that results of edge- and line detection with and without speckle reduction are complementary. When applying the detectors directly to the SAR images, large scanning rectangles have to be used because of the presence of speckle. This allows a detection of low-contrasted lines but gives a poor spatial accuracy. If a speckle reduction is applied before the line detection, smaller scanning rectangles can be used and structures are localised more precisely. In fig. 4 results of applying both methods to a full-polarimetric L-band E-SAR image, using the Hotellings test-based line detector, are shown. On the right figure, showing the line detection results after speckle reduction, the details of the shadow and road structure are much clearer than on the middle one, which represents the results without speckle reduction.

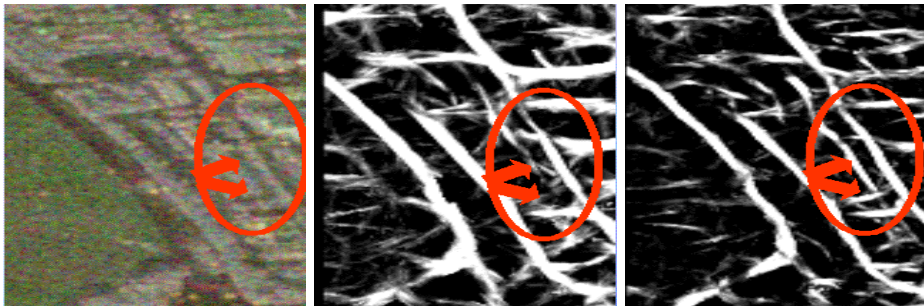


Figure 4. Results of line detection: Left: Original image (L-band, full-polarimetric E-SAR image ©DLR), Centre: results of line detection without speckle reduction, Right: of line detection after speckle reduction

On the other hand different frequencies provide different information about the scene. Therefore we need to find a method to combine the line-detection information from different frequency bands, with and without the use of speckle reduction. By combining the geocoding matrices from the different bands it is possible to find the relationship between the positions in the different images. However, because of the difference in spatial resolution, this is not a one-to-one relationship. This is why we decided to apply the raw line detector to each

band separately and combine only the results. Figure 5 presents a general overview of the adopted line detection strategy.

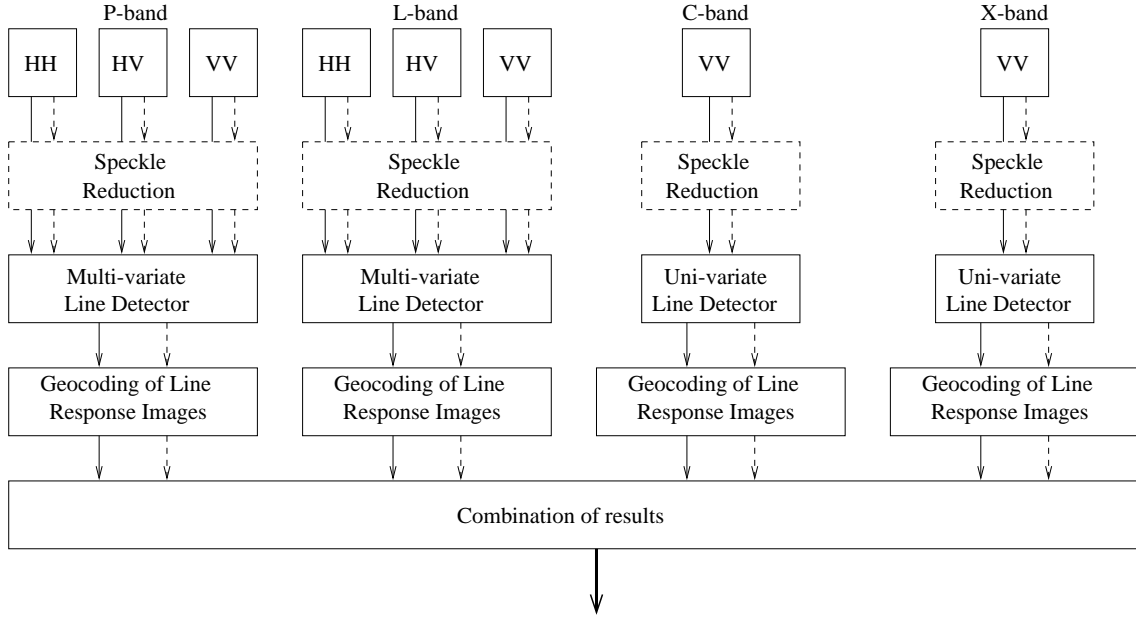


Figure 5. Strategy proposed for line detection in multi-channel SAR images

The different detectors that are used are summarised in table 5.1. Depending on the detector that will be used the SAR SLC image is transformed to an intensity or log-intensity image.

Image Type	Speckle Reduction ?	Image Format	Detector
Pband, Polarimetric	N	Log-Int	Hotellings
	Y	Log-Int	Hotellings
Lband, Polarimetric	N	Log-Int	Hotellings
	Y	Log-Int	Hotellings
Cband, VV	N	Intensity	Touzi
	Y	Log-Int	Student
Xband, VV	N	Intensity	Touzi
	Y	Log-Int	Student

Table 3. Overview of the detectors used for different images, with and without speckle reduction

5.2. Combination of the results

Before being able to combine the results, they need to be transformed into a common coordinate system. We use the geocoding matrices to warp all results into geocoded coordinates. Because of the difference in azimuth resolution of the different images the mapping is not one-to-one. The geocoded coordinates can correspond to different coordinates in the slant-range image. In this case we use the maximum of these for the line strength image and use the position of this maximum for finding the corresponding line direction.

Because the results of different detectors need to be combined, it is necessary to rescale the line strength results first. This rescaling is done such that the same pixel value in the different images corresponds to the

same probability of false alarms. Although theoretically it should be possible to determine the rescaling function from the p-values of the various detectors, it is very difficult to model the influence of spatial correlation in the image and the effect of the speckle reduction. Therefore we derived the rescaling function empirically.

The line direction images obtained in the different bands or for the different methods are used to determine a measure of average distance and standard deviation in edge-direction estimations at each pixel. This standard deviation is then used as a weighing factor for the line strength images.

The actual fusion (combination) is just a sum for the moment, but other methods^{12, 13} will be investigated later. Fig. figure:FuseMethod represents the combination method schematically.

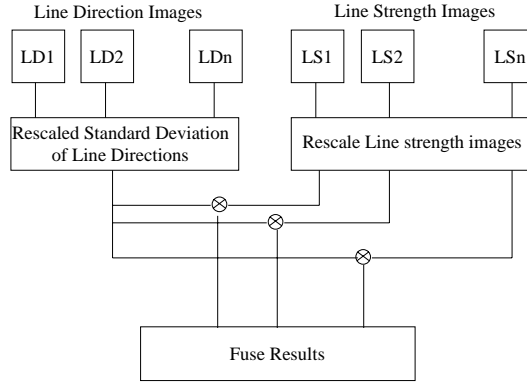


Figure 6. Overview of the method used for combining the results

6. EVALUATION METHOD

The results of the line detectors are evaluated using ROC curves which represent the probability of detection P_d as a function of probability of false alarms P_f . The curves are generated by varying the detector's threshold. In order to determine these curves the ground-truth for dark and bright lines was manually indicated on a part of a geocoded high-resolution visual image (an image of the Daedalus line-scanner, provided to us by DLR). For bright lines we indicated lines of trees and bushes on the image, for dark lines roads, paths and rivers were indicated. In order to determine the ROC curves we need to find the probability of detection and the probability of false alarms. As we wish to evaluate the raw results of the detectors and because they give a relatively wide response to a line, this is not straightforward. We have chosen the following definitions:

- *Probability of Detection (P_d)*: For a given detector threshold this is based on the number of pixels in the detector's result image for which the value is above the threshold and the position is within a given distance of the line ($D \leq \Delta_{max}$). P_d is then defined as the number of detections along the true line divided by the number of pixels of the true line
- *Probability of False Alarms (P_{fa})* is defined as the number of pixels above a given threshold that are not within a given distance ($D > \Delta_{min}$) from a true line divided by the total number of pixels in the image that are not within the defined distance from any true line.

Because of the SAR image acquisition geometry and the fact that edges of trees are shifted in SAR images w.r.t. their position on a visual image, the distance thresholds have to be taken quite high. We used $\Delta_{max} = 20m$, $\Delta_{min} = 30m$. This could underestimate the probability of false alarms. Note also that for dark lines, the ground-truth only contains roads and rivers whereas the line detector in SAR will also detect shadows of forests, buildings and lines of trees or bushes. For the bright lines the detector also finds delimitations made by bricks on the ground or walls. These are not included in the ground-truth either. The ROC curves therefore allow to compare different detectors among them but the absolute result should be interpreted with care. Note also that the evaluation method described here does not take into account spatial accuracy. A method for evaluating this is under development.

7. RESULTS AND DISCUSSION

The line detection scheme was applied to all available images with and without applying speckle reduction. Two window sizes for the scanning windows were used for both cases. For the line detection applied on the original image sizes of resp. 5×30 and 10×30 were used. For the detection after speckle reduction sizes 5×10 and 3×20 were used. The methods were applied to find resp. dark and bright lines.

Fig. 7 shows the ROC curves for the detection of bright lines using P-band (left) and L-band (right). The curves show the results with and without speckle reduction and each time for two different window sizes. For both bands the global results after speckle reduction are better than without speckle reduction. The L-band gives a higher probability of detection than the P-band images. This could be due to the fact that some of the bright lines in the ground-truth are low bushes. These would be more transparent for P-band than for L-band SAR.

Fig. 8(left) shows the ROC curve for the detection of bright lines for all bands after speckle reduction and with a window size of 5×10 . Apparently L-, C- and X-band give similar results for the detection of bright lines. However, because of the SAR image acquisition physics, the position of the bright lines corresponding to treelines depends on the wavelength of the radar. Therefore, when filtering using edge direction variance, we need to consider results obtained for different bands separately. We grouped P- and L-band results on one hand and C- and X-band results on the other hand. The figure also shows the result after applying the fusion scheme. Even with the simple fusion method (the sum) results after fusion are better than the results of any individual band for the detection of bright lines.

The middle picture in fig. 8 presents the ROC curve for detection of bright lines using the L-band speckle reduced image, before and after the weighting with the standard deviation of edge directions, obtained from P- and L-band. The rescaling improves results slightly by reducing the edge strength of the false alarms.

Fig. 8(right) gives the results for the detection of dark lines using the speckle reduced images of the 4 bands. This time the ROC curves for the different frequencies intersect each other. This means that the results from the different bands are complementary. The L- and P-band globally give the best results at low false alarm rates while P-band does not allow to achieve the probability of detection that the other bands do at higher false alarm rate. This could be due to the smaller spatial resolution of the P-band images. This time the ROC curve for the result after fusion is in the middle of those obtained from the different bands. This can mean that the fusion method needs to be improved. A reason for this degraded performance can be the following: In L-band the roads and rivers are visible while the shadows are not that pronounced. In C- and X-band the shadows are very well visible. This means that fusing L-band with C- and X-band increases the number of false alarms due to shadows. If the shadows could be identified among the detected bright lines, the problem could be solved.

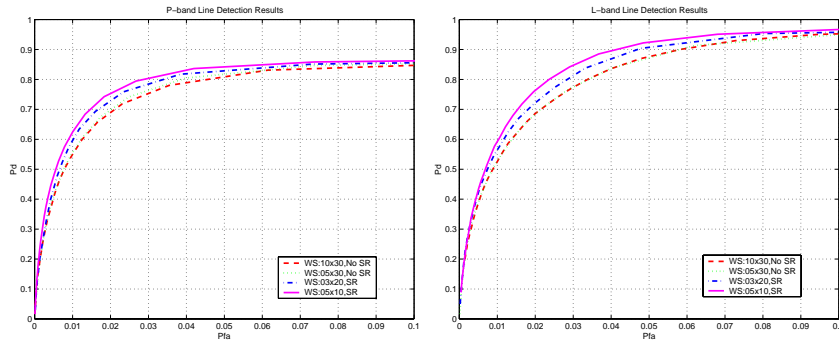


Figure 7. ROC curves for the detection of bright lines for P- and L-band with and without speckle reduction (SR)

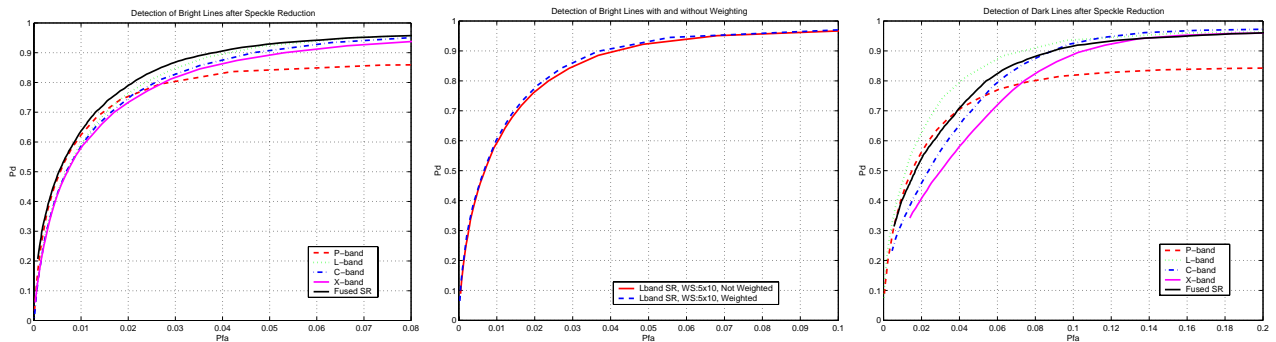


Figure 8. ROC curves for the detection of bright lines for all bands after speckle reduction (left) and before and after rescaling the results for L-band, speckle reduced images (with $WS:5 \times 10$), Right: the same as left but for detection of dark lines.

Fig. 9 shows the global results that were obtained. In the left figure the results after fusion of the dark and bright line detectors are shown, on the left the ground truth objects are shown. They contain roads, paths, rivers and lines of trees and bushes.

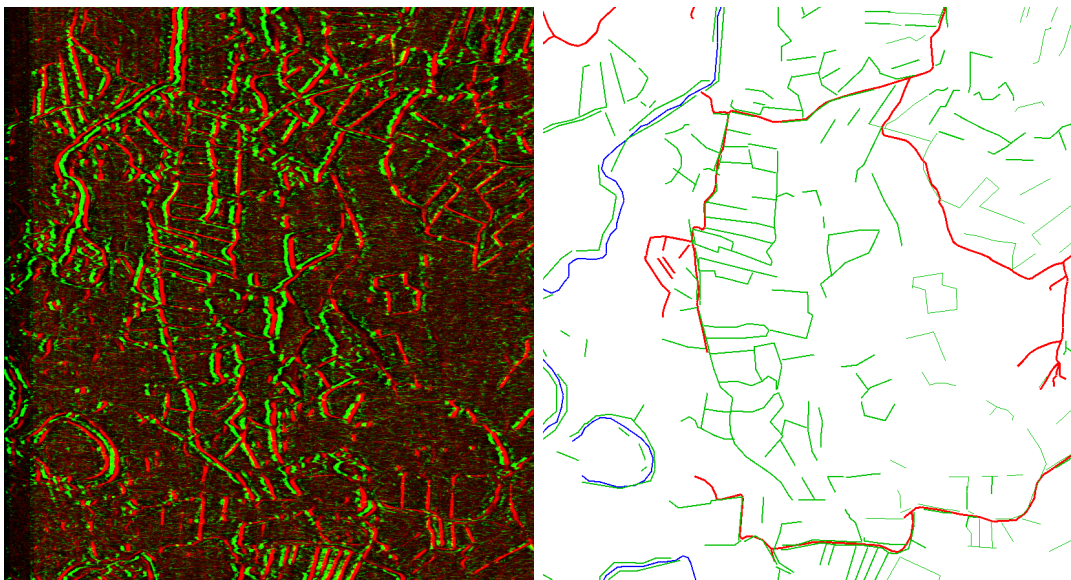


Figure 9. Global results. Left: detected dark (green) and bright (red) lines, Right: ground truth containing treelines (green), rivers (blue) and roads (red).

8. CONCLUSIONS AND FURTHER WORK

In this article a method for detection of linear objects in multi-channel SAR images was proposed. The method was applied on a set of SAR images consisting of P- and L-band full-polarimetric images and VV-polarised C- and X-band images. Because of the difference in spatial resolution and information content of the 4 frequency bands, results are improved by fusing the individual results from the different bands. The influence of applying speckle reduction prior to line detection was also studied. The results after speckle reduction are globally better than those without speckle reduction. Three different line detectors were applied according the type of image that is treated. For full-polarimetric images a detector based on multi-variate statistics is used, for the original

single-polarisation images the Touzi detector was used and for the speckle reduced single-polarisation images a statistical method based on a Student-t test was used. A fusion scheme was proposed to combine the results from different bands with and without speckle reduction. Although the proposed fusion method is very simple, results after fusion are better than those obtained by any of the single bands. Ground truth for evaluation was extracted from a high-resolution visual image of the same region. ROC curves are shown to evaluate the different steps in the algorithm. For detection of bright lines (treelines) the method gives very good results. For the detection of dark lines the method still needs some improvement. In particular a better fusion method will need to be developed. On the other hand the detector of dark lines detects roads, rivers but also shadows from forests, treelines and buildings. We need to develop a method to distinguish between these. Classification results, either from the SAR images or from visual images of the same scene could help here.

ACKNOWLEDGMENTS

The research presented in this paper is the result of a collaboration between two projects: ASARTECH: “Advanced SAR Technologies”, funded by the Belgian Government, Belgian Federal Science Policy Office, in the frame of the STEREO Program (project nr. SR/00/04) and SMART: “Space and airborne Mined Area Reduction Tools”, funded by the European Commission (project nr. IST-2000-25044).

REFERENCES

1. F. Tupin, H. Maître, J. Mangin, J. Nicolas, and E. Pechersky, “Detection of linear features in sar images: Application to road network extraction,” *IEEE-GRS* **36**, pp. 434–453, March 1998.
2. O. Hellwich, H. Mayer, and G. Winkler, “Detection of lines sar scenes,” in *Proc. ISPRS Workshop*, vol. 31, pp. 312–320, (Vienna, Austria), 1996.
3. D. Borghys, V. Lacroix, and C. Perneel, “Edge and line detection in polarimetric sar images,” in *International Conference on Pattern Recognition, Quebec*, vol. 2, pp. 921–924, Aug 2002.
4. A. Pizurica, W. Philips, I. Lemahieu, and M. Acheroy, “Despeckling sar images using wavelets and a new class of adaptive shrinkage estimators,” in *Proc. IEEE Conf. on Image Proc. (ICIP)*, (Thessaloniki, Greece), Oct 2001.
5. F. Tupin, *Reconnaissance des Formes et Analyse de Scènes en Imagerie Radar à Ouverture Synthétique*. PhD thesis, ENST, Paris, September 1997.
6. A. Bovik, “On detecting edges in speckle imagery,” *IEEE-ASSP* **36**, pp. 1618–1626, October 1988.
7. R. Touzi, A. Lopes, and P. Bousquet, “A statistical and geometrical edge detector for sar images,” *IEEE-GRS* **26**, pp. 764–773, November 1988.
8. D. Borghys, C. Perneel, and M. Acheroy, “A multi-variate contour detector for high-resolution polarimetric sar images,” in *International Conference on Pattern Recognition, Barcelona*, vol. 3, pp. 650–655, sept 2000.
9. D. Borghys, *Interpretation and Registration of High-Resolution Polarimetric SAR Images*. PhD thesis, ENST E 031, Paris, Nov 2001.
10. A. Pizurica, *Image Denoising using Wavelets and Spatial Context Modeling*. PhD thesis, University of Ghent, Faculty of Applied Sciences, Department of Telecommunications and Information Processing, June 2002.
11. A. Lopes, E. Nezry, R. Touzi, and H. Laur, “Structure detection and statistical adaptive speckle filtering in sar images,” *Int. J. Remote Sensing* **14**, pp. 1735–1758, May 1993.
12. I. Bloch, “Information combination operators for data fusion: A comparative review with classification,” *IEEE-SMC(Part A)* **26**, pp. 52–67, January 1996.
13. J. Chanussot, G. Mauris, and P. Lambert, “Fuzzy fusion techniques for linear features detection in multi-temporal sar images,” *IEEE-GRS* **37**, pp. 1292–1305, May 1999.